Hydrogen peroxide oxidation of $Fe_2(ttha)^{2-}$: a path different from autoxidation

Songsheng Zhang, Kathleen S. Snyder and Rex E. Shepherd*
Department of Chemistry, University of Pittsburgh, Pittsburgh, PA 15260 (USA)

(Received June 24, 1991; revised June 8, 1992)

Abstract

$Fe^{II}_2(ttha)(H_2O)_2^{2-}$ is oxidized rapidly by H_2O_2, but greater than a 1:1 stoichiometric consumption of H_2O_2 occurs. While the oxidation product of $O_2/Fe_2(ttha)(H_2O)_2^{2-}$ is greater than 95% $Fe_2O(ttha)^{2-}$, the H_2O_2 oxidation products include *c.* 80% $Fe^{III}_2O(ttha)^{2-}$, *c.* 20% of a tetranuclear complex $Fe^{III}_4(O)_2(ttha)_2^{4-}$, and traces of $Fe^{III}Cl_4^-$ and $Fe^{III}(tthaH)^{2-}$. The $Fe^{II}_2(ttha)(H_2O)_2^{2-}$ oxidation by H_2O_2 exhibits only a 6.8% suppression in the presence of 0.10 M t-butanol instead of a 50% suppression if production of HO· is a major pathway in the H_2O_2 oxidation. The mechanism is proposed to occur via formation of ferryl intermediates which may react with the second iron(II) site within the same molecule by an inner-sphere route forming the μ-oxo bridged $Fe^{III}_2O(ttha)^{2-}$ or by outer-sphere electron transfer forming an open-chain $Fe^{III}_2(ttha)(H_2O)_2$ complex. The same ferryl intermediate may react inner-sphere with a second $Fe^{III}_2(ttha)(H_2O)_2^{2-}$ complex, leading to the tetranuclear product. The pathways which yield $Fe_2O(ttha)^{2-}$ upon ring closure of open-chain $Fe^{III}_2(ttha)(H_2O)_2$ involve three parallel pathways utilizing aqua/aqua, aqua/hydroxy and hydroxyl/hydroxy forms of $[Fe^{III}_2(ttha)]$ with first-order rate constants of 12.0, 11.6 and 0.11 s^{-1}, respectively ($\mu=0.05$, $T=25.0$ °C). The abnormally high reactivity of the aqua–aqua species for μ-oxo formation is consistent with a hydrogen-bonded orientation of $Fe^{III}_2(ttha)(OH_2)_2$ within its own solvent cage which places the Fe^{III} centers close for μ-oxo formation. A peroxo complex forms via substitution at a terminal site of $Fe^{III}_2(OH)_2^{2-}$ with a second-order rate constant of 4.32 ± 0.20 M^{-1} s^{-1}. A slower first-order rearrangement of the initial peroxo adduct is observed ($k=0.14\pm0.02$ s^{-1}) with an $[H_2O_2]$-independent rate. A rearrangement from an initial η^2-peroxo coordination to an $\eta^1{:}\eta^1$ (bridged) coordination is proposed. The peroxo species of $[Fe^{III}_2(ttha)]$ which is isolated by ethanol-induced precipitation from solution containing 13.6:1.0 $H_2O_2{:}Fe^{III}_2(ttha)(H_2O)_2$ exhibits a new band at 791 cm^{-1}, consistent with $\eta^1{:}\eta^1$ coordination based on $[Co^{III}_2(H_2O)_2(O_2)(histidinate)_4]$ as a model. Although the η^2-peroxo complex $[Fe^{III}(O_2)(edta)]^{3-}$ exhibits a purple color due to an LMCT band at 528 nm, neither $[Fe_2(O_2)(ttha)]^{2-}$, nor $[Fe^{III}(hedta)(O_2)]^{2-}$ possess a band above 500 nm, a feature frequently attributed as diagnostic of ferric peroxo species with polyaminopolycarboxylate ligands. $[Fe^{III}(hedta)(O_2)]^{2-}$ is observed to be golden-brown at pH 10.30 and to have the anticipated $\nu(OO)$ stretch at 810 cm^{-1} for the η^2-peroxo complex. Yet it has no LMCT band above 440 nm.

Introduction

Numerous biological and industrial processes require oxygen activation by transition metal complexes in reaction with either O_2 or H_2O_2 [1, 2]. Information concerning both peroxo complexes and higher valent forms of iron is of current importance for understanding beneficial cellular oxidations, particularly from oxygenase and monooxygenase systems, but also for cellular damaging processes such as lipid peroxidation [1, 3, 4]. Many of these processes involve non-heme iron proteins. For this reason there is an interest in the reactions of $Fe^{II/III}$ complexes with O_2 and H_2O_2 in which the iron centers are ligated by donors available in proteins. There is an active search for functional and model systems which activate either H_2O_2 or O_2 for subsequent organic oxidations. Several catalytic systems which utilize pyridine carboxylates for the oxidation of organic substrates have been recently described by Sawyer [1d] and the nitrilotriacetate Fe^{III} complex has been examined as a model for catechol dioxygenases by Fujii *et al.* [1d].

The amine and carboxylate donors available with polyaminopolycarboxylate ligands (pacs) related to $edta^{4-}$ offer a chemical environment similar to metalloprotein binding sites. Studies or redox reactions with $Fe^{II/III}$(pacs) with O_2, O_2^-, H_2O_2 and RC(O)(OOH) have been made by various research groups [5–9], but these reports have been limited in all but one case of $Fe^{II/III}$(pacs) having mononuclear complexation. A recent study from our laboratory of the autoxidation of the diiron $Fe^{II}_2(ttha)(H_2O)_2^{2-}$ complex ($ttha^{6-}$ =

*Author to whom correspondence should be addressed.

0020-1693/92/$5.00

triethylenetetraaminehexaacetate) has shown that the presence of a second metal center, maintained in close proximity to the first, imparts major changes in the course of reduction of O_2 [10]. Dissociation of H_2O_2, an important step in the autoxidation of mononuclear Fe^{II}(pacs) [11], is by-passed for O-atom transfer as a more direct reduction pathway [10] with $Fe^{II}_2(ttha)(H_2O)_2^{2-}/O_2$.

Fe^{II}–pac autoxidations [12, 13] were reassessed recently by Zang and van Eldik for $Fe^{II}L$ ($L = edta^{4-}$, $hedta^{3-}$ and $dtpa^{5-}$) [11]. Fe^{II}–pac/O_2 reactions proceed by sequential $1e^-$ reductions involving an Fe^{III}–superoxo intermediate, $[LFe^{III}(O_2^-)]$ [11]. This species has also been detected by a spin-trapping study from our laboratory*. At high $[Fe^{II}L]$ the rate law for autoxidation obeys a $[Fe^{II}L]^2$ relationship which was interpreted by van Eldik as evidence for the inner-sphere reduction of $[LFe^{III}(O_2^-)]$ by $Fe^{II}L$, forming an $\eta^1{:}\eta^1$ bridged peroxo complex, $LFe^{III}(O_2)Fe^{III}L$.

$LFe^{III}(O_2)Fe^{III}L$ complexes of van Eldik's scheme undergo rapid proton-assisted dissociation and are not isolable. Diferric peroxo complexes, stabilized by binucleating ligands have been reported with the HPTB and 5-MeHXTA type of ligands [14]. The $\eta^1{:}\eta^1$ diferric peroxo complexes are believed to be inherently unstable with respect to cleavage with metal oxo formation [3, 15, 16]. However, Sawyer *et al.* have invoked diferric peroxo complexes as active oxygenating intermediates with both dioxygenase and monoxygenase character using the bis-picolinate or bis-2,6-dicarboxylatopyridine iron catalysts for the oxidation of both saturated and unsaturated hydrocarbons in dimethylformamide as a solvent [17]. Hence the favorability of diferric peroxo species may be highly solvent dependent, or dependent on the propensity of the ligand structure to facilitate adjacent iron centers.

The oxidation of Fe^{II}–pacs by H_2O_2 has been shown to proceed by a somewhat unanticipated mechanism [18, 19]. It has been known for many years that the combination of $Fe^{II}(edta)^{2-}$ with H_2O_2 (Fenton's reagent) would serve as a source of oxidizing power for organic substrates that has all of the properties attributable to the hydroxyl radical ($HO^\cdot$) [20]. Although $HO^\cdot$ is readily detectable in $Fe^{II}(pac)/H_2O_2$ reactions*, Rush and Koppenol [18, 19] have shown that $HO^\cdot$ production occurs as a secondary reaction pathway (eqn. (5) of Scheme 1), and not by a direct $1e^-$ route (eqn. (1)). The main reaction sequence involves a $2e^-$ oxidation of $Fe^{II}L$ by H_2O_2 resulting in a ferryl intermediate which may be formulated as $LFe^{IV}O$ (L = pac), eqns. (2)–(8) of Scheme 1. $LFe^{IV}O$ and $HO^\cdot$ behave

$$Fe^{II}L + H_2O_2 \longrightarrow Fe^{III}L + OH^- + HO^\cdot \quad (1)$$

$$LFe^{II} + H_2O_2 \longrightarrow LFe^{IV}O + H_2O \quad (2)$$

$$LFe^{IV}O + LFe^{II} \longrightarrow 2LFe^{III} \quad (3)$$

$$LFe^{IV}O + H_2O_2 \longrightarrow LFe^{II} + O_2 + H_2O \quad (4)$$

$$LFe^{IV}O + H_2O_2 \longrightarrow LFe^{III}(O_2H^-) + HO^\cdot \quad (5)$$

$$HO^\cdot + LFe^{II} \longrightarrow LFe^{III} + OH^- \quad (6)$$

$$HO^\cdot + RH \longrightarrow R^\cdot + H_2O \quad (7)$$

$$LFe^{IV}O + RH \longrightarrow LFe^{III}(OH^-) + R^\cdot \quad (8)$$

Scheme 1.

in a kinetically equivalent manner for the oxidation of primary and secondary alcohols when these are present with $Fe^{II}(pac)/H_2O_2$ solutions (eqns. (7) and (8)). However, t-butanol also is oxidized by $HO^\cdot$, but not by $LFe^{IV}O$, differentiating between $HO^\cdot$ and $LFe^{IV}O$ [18]. Examination of the data of Rush and Koppenol for $Fe(edta)^{2-}/H_2O_2$ suggests that $HO^\cdot$ is formed about 5.4% of the time via eqn. (5) while pathway (3) accounts for about 80% of redox events for $LFe^{IV}O$ [18]. The observations of Rush and Koppenol have proven important for the interpretation of the multistep oxidation of $Fe^{II}_2(ttha)(H_2O)_2$ by H_2O_2, which is reported in the present paper. Two different μ-oxo products are observed. One of these occurs from 'self-reaction' by inner-sphere redox between the separate iron sites of $Fe_2(ttha)^{n-}$ and another product by cross-polymerization during intermolecular redox with another $Fe_2(ttha)(H_2O)_2^{2-}$. The latter leads to a tetranuclear iron complex.

We have also observed a further reaction with $Fe^{III}_2(ttha)(H_2O)_2$ at high $[H_2O_2]$ (≥ 0.10 M), indicative of peroxo coordination. The product may provide a model for the $\eta^1{:}\eta^1$-bridged intermediate proposed for O_2 oxidation of Fe^{II}(pacs) [11]. The spectral nature of the peroxo complex formed at high $[H_2O_2]$ with $[Fe^{III}_2(ttha)(H_2O)_2]$ is different from the well-known purple complex $[Fe^{III}(edta)(O_2)]^{3-}$ which has recently been characterized as an η^2-peroxo complex [21–24] having an $Fe^{III} \leftarrow O_2^{2-}$ LMCT band at *c.* 520 nm. It is shown here that Fe^{III}–peroxo complexes in pac ligand environments may have $Fe^{III} \leftarrow O_2^{2-}$ LMCT transitions at higher energies than commonly assumed on the basis of a limited number of prior literature reports [25].

Experimental

Reagents

Triethylenetetraaminehexaacetic acid, H_6ttha, and tris(hydroxymethyl)aminomethane (tris buffer) were ob-

*References 10 and 11 show that the autoxidation process is on the stopped-flow time scale; no change in the final absorbance occurs with continued oxygenation for over an hour.

tained from Sigma. *N*-Hydroxyethylethylenediamine-triacetic acid was obtained from Aldrich. Borate buffer (pH = 9.18) was prepared from Fisher Scientific preweighed packages. Acetate and formate buffers were prepared by titration of Mallinckrodt analytical reagent (AR) grade glacial acetic and formic acids with NaOH. 2,6-Lutidine, obtained from Aldrich, was distilled under reduced pressure in all glass apparatus. $Fe(NH_4)_2(SO_4)_2 \cdot 6H_2O$ and $FeCl_2 \cdot 4H_2O$ were obtained from J. T. Baker Chemical Company as analytical grade reagents. O_2 and Ar gases were supplied by Air Products. Traces of O_2 in Ar blanketing gas were removed by passage of the gas through Cr(II) scrubbing towers, followed by an H_2O rinse tower. H_2O_2 was obtained as a 3% solution from EM Industries or J. T. Baker; its actual H_2O_2 titre was determined by standardization with $Ce(NH_4)(SO_4)_2$ standard solution in 2 M H_2SO_4. $(CH_3)_3COOH$ was obtained from Aldrich.

Methods

Transfers of air-sensitive solutions were carried out with gastight syringe techniques, using stainless steel needles. The $Fe_2(ttha)(H_2O)_2^{2-}$ solutions were prepared by dissolving weighed amounts of H_6ttha and adjusting the pH to a desired value prior to purging the solution of O_2 by the Ar blanketing gas. Samples were prepared in bubblers which were connected to the main Ar line with glass ball and socket joints; reagent reservoirs were vented through needles in rubber septa which sealed the flasks. Additions of the proper amount of $Fe(NH_4)_2(SO_4)_2 \cdot 6H_2O$ in polyethylene boats were made rapidly while maintaining an Ar positive pressure. The pH was monitored continuously by a minicombination glass/SCE electrode which was mounted in one neck of the reaction bubbler flask. The pH electrode was calibrated at room temperature against Fisher Scientific gram-pac buffers at convenient values (4.01, 6.86, 9.18). Reagent buffers were prepared by combining weighed amounts of 2,6-lutidine with 1.00 M $HClO_4$ to provide stock lutidine/lutidinium ion buffer at pH = 7.00 or weighed amounts of tris with either NaOH or $HClO_4$ to obtain a pH = 7.50 buffer. The electrolyte concentration was chosen to be 0.050 M with buffers assuming this role; unbuffered systems were also made 0.050 M in ionic strength with $NaClO_4$. pH measurements were made on a digital Fisher 801 pH meter. UV–Vis spectral data were recorded on a Varian-Cary 118C spectrophotometer in 1.00 cm quartz cells. The cells were sealed with rubber septa and flushed with Ar for samples needing protection from O_2. The Ar flushed cells were filled with appropriate solutions by syringe techniques.

Studies of the IR spectra of products obtained under different $Fe^{II}_2(ttha)(H_2O)_2^{2-}$:$H_2O_2$ ratios as a function of time required a rapid isolation of the $[Fe_2(ttha)]$ species from solution. Procedures found to be acceptable in the prior study of the O_2 oxidation of $Fe^{II}_2(ttha)(H_2O)_2^{2-}$ were used to isolate solids at appropriate reaction times [10]. The source of iron for the IR studies was $FeCl_2 \cdot 4H_2O$ to avoid bands due to NH_4^+ or SO_4^{2-}. Rapid addition of ethanol promotes precipitation from solution of the $[Fe_2(ttha)]^{n-}$ complexes as their Na^+ or K^+ salts. The precipitated salts were filtered and dried overnight in a vacuum oven at 35 °C. The dried solids were then ground with KBr and pressed at 9 tons pressure into IR pellets. IR spectra were obtained with an FT-IR device (Perkin-Elmer 32 FTIR) using an average of 64 scans. Calibration of the UV–Vis and IR spectra of the Fe^{III} products formed by either H_2O_2 or O_2 oxidation of $Fe^{II}_2(ttha)(H_2O)_2^{2-}$ was made using weighed amounts of the $[Me_2Dabco][Fe_2O(ttha)] \cdot 6H_2O$ salt [10] ($\lambda_{max} = 470$ nm, $\epsilon/Fe^{III} = 64.0$ M^{-1} cm^{-1}). For studies which evaluated the amount of $Fe_2O(ttha)^{2-}$ product versus other peroxo or open-chain Fe^{III} complexes which are produced, the 836 cm^{-1} band which has been assigned to the Fe–O–Fe assymetric stretch [10, 26, 27] was carefully examined. Since every binuclear iron–ttha species has the same number of carboxylate donors (six from the $ttha^{6-}$), the ν(COOM) vibration at 1632 cm^{-1} was utilized as an internal standard for variations in the intensity in the 836 cm^{-1} region.

Stopped-flow data were collected on a Durrum D-110 stopped-flow spectrophotometer interfaced with a DEC-1103 computer for data analysis*. Ring-closure and ring-opening experiments were carried out by the pH-jump technique and monitored at 470 nm. The stopped-flow pathlength is 2.00 cm. Data reduction and analysis were achieved with appropriate first-order kinetic programs. Reactions were followed for 7 half-lives. In the case of sequential reactions the first reaction was treated with a kinetic program which seeks the best fit using a reiterated first A_∞ value. The second reaction was followed at longer times such that the first reaction component had decreased significantly.

Results and discussion

Product of O_2 oxidation of $Fe^{II}_2(ttha)(H_2O)_2^{2-}$

The prior study of the kinetics of the $Fe^{II}_2(ttha)(H_2O)_2^{2-}/O_2$ reaction was carried out in unbuffered media [10]. The autoxidation process (eqn. (9)) should proceed with no pH changes. However,

*Error estimates given for the rate constants from stopped-flow data are expressed as the average deviation from the mean. Error estimates on derived kinetic constants are those of the least-squares fit to the observed kinetic data.

$$2Fe_2(ttha)(H_2O)_2^{2-} + O_2 \longrightarrow 2Fe_2O(ttha)^{2-} + 4H_2O \quad (9)$$

it was deemed important for studies of the H_2O_2 oxidation to show that reaction (9) was independent of pH or the buffer media supplying the pH control. Additionally, since buffer components in 2,6-lutidine or tris are weakly capable of metal ion coordination, it was necessary to show that the products obtained are independent of the buffer media. Three 4.00×10^{-3} M solutions of the $Fe^{II}_2(ttha)(H_2O)_2^{2-}$ complex were prepared in 0.050 M lutidine/lutidinium perchlorate buffer (pH = 7.00), tris/trisH$^+$ buffer (pH = 7.50) and unbuffered pH (adjusted to 6.88 $\mu = 0.05$ with $NaClO_4$). The three separate samples were bubbled with O_2 vigorously for 9 min and yielded identical spectra (Fig. S1, see 'Supplementary material'.) The pH of the reaction solutions remained unchanged for both the buffered and the unbuffered systems at their respective pH. The spectrum obtained for each product solution matched the spectrum of an equivalent 4.00×10^{-3} M solution obtained by dissolving the analyzed [Me_2Dabco]-[$Fe_2O(ttha)$]·$6H_2O$ salt. This confirms that only the μ-oxo complex is produced by the O_2 oxidation pathway [10].

H_2O_2 oxidation of $Fe_2(ttha)(H_2O)_2^{2-}$

The oxidation of $Fe^{II}_2(ttha)(H_2O)_2^{2-}$ was observed to proceed with H_2O_2 in either unbuffered solution, pH = 7.32, or in 2,6-lutidine/lutidinium perchlorate, pH = 7.00, with identical results. The spectra obtained for the oxidation of 3.98×10^{-3} M $Fe^{II}_2(ttha)(H_2O)_2^{2-}$ in 0.05 M lutidine buffer are shown in Fig. 1. Curve A shows the spectrum of $Fe_2O(ttha)^{2-}$ produced by O_2 oxidation of the same solution as a control, indicative of the total amount of the μ-oxo-bridged complex available upon oxidation of all Fe^{II} in the system. A separate ion exchange study showed that greater than 95% of the product formed by O_2 oxidation of $Fe^{II}_2(ttha)(H_2O)_2^{2-}$ is the single 2-anionic species, $Fe_2O(ttha)^{2-}$. Curve B shows the UV–Vis spectrum under Ar at a $Fe^{II}_2(ttha)(H_2O)_2^{2-}$:$H_2O_2$ ratio of 1:1 while C is at 1:2, D is at 1:11.8. Spectrum E is obtained from solution B which has been treated with O_2 saturation by bubbling for 12 min after the initial reaction at 1:1 H_2O_2. The spectrum obtained for B is below that of A. The analysis under conditions for E and the known ϵ for $Fe_2O(ttha)^{2-}$ at 470 nm allows the calculation of an effective ϵ/Fe of 72.5 M^{-1} cm^{-1} under conditions of H_2O_2 at 1:1. The effective ϵ_{470} when Fe^{II} is totally oxidized at either 1:2 or 1:11.8 H_2O_2 is found to be nearly the same (71.5 M^{-1} cm^{-1}). This value is higher than that observed for $Fe_2O(ttha)^{2-}$ ($\epsilon_{470} = 64.0$ M^{-1} cm^{-1}). The amount of unreacted Fe^{II}, which is detected by the second O_2 oxidation converting spectrum B to E, was also evaluated in a separate experiment using 2,2′-bipyridine (bpy) as a scavenger for unreacted Fe^{II} in the system with equivalent results.

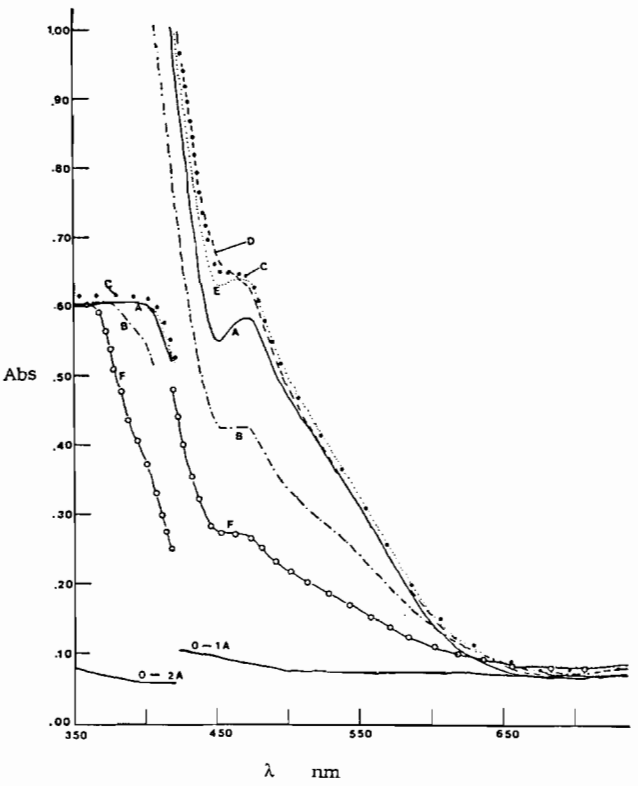

Fig. 1. H_2O_2 and O_2 oxidations of $Fe_2(ttha)(H_2O)_2^{2-}$. $[Fe^{II}_2(ttha)(H_2O)_2^{2-}]_{initial} = 3.98\times10^{-3}$ M in 0.050 M lutidine/lutidinium perchlorate buffer (pH 7.00) (A) complete O_2 oxidation at 45 min. (B) 4.17×10^{-3} M H_2O_2 added. (C) 8.34×10^{-3} M H_2O_2 added. (D) 0.187 M H_2O_2 added (spectra B–C at 10 min under Ar). (E) Sample B bubbled with O_2 for 12 min. (F) 2.08×10^{-3} M H_2O_2 added under Ar; 1.00 cm cell.

If HO$^\bullet$ were formed during the oxidation of $Fe^{II}_2(ttha)(H_2O)_2^{2-}$ it should be completely scavenged by 0.10 t-butanol [18]. The oxidation of $Fe^{II}_2(ttha)(H_2O)_2^{2-}$ by O_2 and H_2O_2 oxidants is presented in Fig. 2. The presence or absence of 0.10 M t-butanol has no effect on the $Fe^{II}_2(ttha)(H_2O)_2^{2-}$ oxidation by O_2 as shown by coincident spectra for these two conditions in spectrum A. This is in agreement with the prior spin trapping study that no free HO$^\bullet$ is detectable when $Fe^{II}_2(ttha)(H_2O)_2^{2-}$ undergoes autoxidation [10].

When $Fe_2(ttha)(H_2O)_2^{2-}$ is oxidized at 1:1 with H_2O_2 in the presence of 0.10 M t-butanol there is a 6.8% decrease in the absorbance change at 470 nm compared to the same system without t-butanol (spectra D versus C). The remaining Fe^{II} may be further oxidized by O_2 (curves E and F). The suppression by the presence of 0.10 M t-butanol represents a minor effect compared to the 50% decrease [19] in the amount of Fe^{III} oxidized

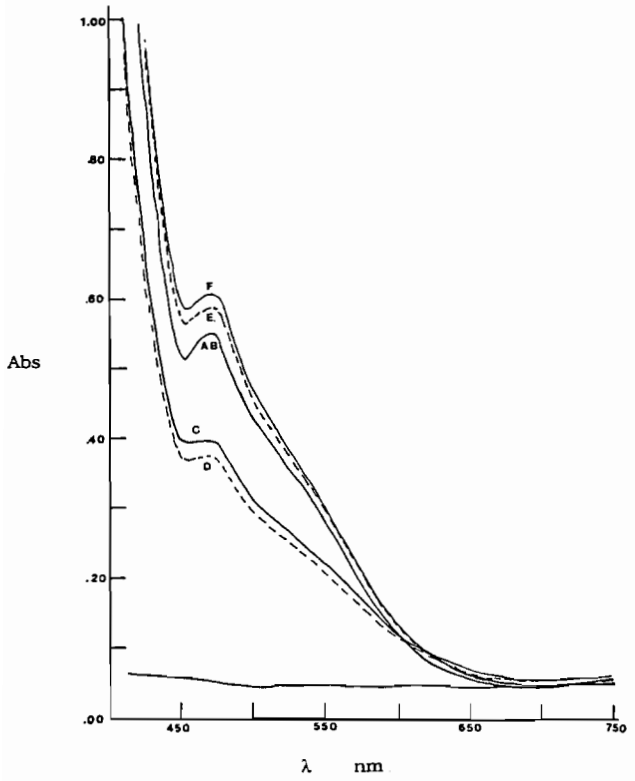

Fig. 2. Effect of t-butanol on $Fe_2O(ttha)^{2-}$ oxidations. $[Fe_2(ttha)^{2-}]_i = 4.00 \times 10^{-3}$ M, pH = 7.00, 0.05 lutidine/lutidinium perchlorate, 1.00 cm cell; (A) and (B), coincident spectra of $Fe_2(ttha)(H_2O)_2^{2-}$ oxidized by O_2 in the presence and absence of 0.10 M t-butanol; (C) $Fe^{II}_2(ttha)(H_2O)_2^{2-}$ under Ar with 4.00×10^{-3} M H_2O_2 added; (D) same as (C) with 0.10 t-butanol added; (E) sample (B) (no t-butanol) further oxidized by O_2; (F) sample (D) further oxidized by O_2.

product if a sequential $1e^-$ oxidation pathway (eqn. (1)) involving the formation of HO· were involved in the main pathway for the H_2O_2 oxidation.

Ion exchange of products of H_2O_2 oxidation

Identical samples of 4.10×10^{-3} M $Fe^{II}_2(ttha)(H_2O)_2^{2-}$ were obtained by splitting of a sample prepared under Ar. Half of the sample was treated with O_2 oxidation. The second half was oxidized with 0.0105 M H_2O_2 (1:2.56 ratio) in order to assure complete oxidation of Fe^{II} to Fe^{III}, but to avoid a large excess of H_2O_2 which promotes further reaction as described in a later section. The two oxidized samples were loaded on identical columns of AG-4X resin in the Cl^- form. The resin was pretreated with HCl and repeatedly washed to reduce hydrogen ion to the neutral pH value. Each sample was then eluted at neutral pH sequentially with 0.10, 0.50, 1.0, 2.0 and 4.0 M NaCl. The sample obtained from O_2 oxidation moved rapidly with 1.0 M NaCl, indicative of a 2^- ion. The spectrum was identical to the solution in the absence of ion exchange when corrected in intensity for column broadening during chromatography. Less than 5% of the absorbing species were moved by 1.88 M saturated Na_2SO_4, indicative of anions of higher charge.

The sample oxidized by H_2O_2 was treated in the same fashion. A small amount of free Fe^{III} eluted with 0.10 and 0.20 M NaCl as the $FeCl_4^-$ complex. The fraction moved with 1.0 M NaCl with a spectrum similar to that of $Fe_2O(ttha)^{2-}$ containing a trace of $Fe^{III}(tthaH)^{2-}$. The combined amount of 2^- anions represented 80% of the elutable absorbing species at 470 nm. A residual material was clearly present as a band at the top of the column after copious washing with 1.0 M NaCl. This species was not moved with 4.0 M NaCl, but was displaced with 1.88 M Na_2SO_4. The spectral features were the same as those of $Fe_2O(ttha)^{2-}$ except that the 550 nm shoulder is more intense ($\epsilon_{550}/\epsilon_{470} = 0.51$) relative to $Fe_2O(ttha)^{2-}$ ($\epsilon_{550}/\epsilon_{470} = 0.47$). The similarity of all spectral chromophores to that of $Fe_2O(ttha)^{2-}$, but with a 4^- charge, clearly suggests a $[Fe_2O(ttha)]_2^{4-}$ formulation. However, the ϵ/Fe at 470 nm of this species must be greater than that of $Fe_2O(ttha)^{2-}$ in order to obtain an effective ϵ/Fe greater for the overall oxidation of H_2O_2 compared to O_2 as described in the prior section. When a weighted distribution of 80% $Fe_2O(ttha)^{2-}$ and 20% $[Fe_4(O)_2(ttha)_2]^{4-}$ is used to adjust the $\epsilon_{effective}$ value, an ϵ/Fe of 107 M^{-1} cm^{-1} is obtained for tetranuclear species at 470 nm. The logical explanation for the 4^- species is a cross-polymer between two $[Fe^{III}_2(ttha)]$ units via μ-oxo bridges. The effective coordination of the Fe^{III} centers in the tetranuclear complex would be similar to the linear-bridged μ-oxo complex of (hedta)FeOFe(hedta)$^{2-}$ [26] for which ϵ_{470} is 90 M^{-1} cm^{-1} per Fe^{III} [27]. Models prepared of the $[Fe^{III}_2(ttha)^{2-}]$ moieties show that a cross μ-oxo bridged tetranuclear species forms quite easily using linear μ-oxo bridges. The side-by-side arrangement in $Fe_2O(ttha)^{2-}$ requires a bent Fe–O–Fe chromophore. Thus it is reasonable that this charge-transfer based transition could have a lower value for the bent structure of $Fe_2O(ttha)^{2-}$ ($\epsilon = 64$ M^{-1} cm^{-1}/Fe^{III}) compared to more absorbing μ-oxo linear chromophores in $[Fe_4(O)_2(ttha)_2]^{4-}$ ($\epsilon \sim 107$ M^{-1} cm^{-1}).

Slow reaction with H_2O_2

Authentic $Fe_2O(ttha)^{2-}$, supplied as the Me_2Dabco^{2+} salt (3.27×10^{-3} M), reacts very slowly in the presence of 0.234 M H_2O_2 (71.6:1). The minimum at 450 nm disappears with time while the 525 nm shoulder feature steadily decreases (Fig. 3). Both the 450 minimum and 525 shoulder are completely changed after 18.5 h to give a nearly featureless spectrum with a slight shoulder at 455 nm. The spectrum is similar to, but more absorbing than, the spectrum obtained for a mononuclear $Fe^{III}(ttha)^{3-}$ complex (curve G). The final 18.5 h spec-

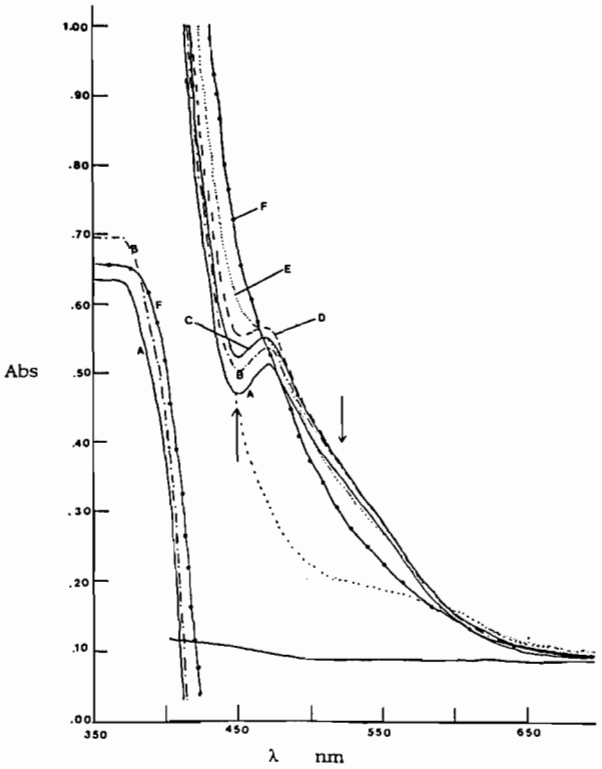

Fig. 3. Slow H_2O_2 reaction with $Fe_2O(ttha)^{2-}$. $[Fe_2O(ttha)^{2-}] = 3.27 \times 10^{-3}$ M in 0.025 M lutidine/lutidinium buffer adjusted to pH = 6.88. (A) Complex in buffer alone, (B) with the same dilutions containing 0.234 M H_2O_2 at 20 min, (C) at 60 min, (D) at 120 min, (E) at 210 min, (F) at 40 h; 1.00 cm cell. (G) Dotted lower curve, 3.96×10^{-3} M $[Fe^{III}(ttha)^{3-}]$ mononuclear complex formed by oxidation with 4.21×10^{-3} M H_2O_2; 1.00 cm cell.

trum remained constant. Changes in the initially formed $Fe_2O(ttha)^{2-}$ occurred with a half-life of *c.* 1.6 h with 0.234 M H_2O_2.

A 3.86×10^{-3} M sample of $Fe_2O(ttha)^{2-}$ was obtained by the O_2 oxidation pathway. The μ-oxo bridge was ruptured by adjustment to a pH at 2.0 [10]. Aliquots adjusted to pH 6.74 and 10.07 were obtained and the respective UV–Vis spectra are shown in Fig. 4, curves A and B. Almost no change is detectable under the two differing conditions of pH. By contrast, it is known that the $[Fe(hedta)]_2O^{2-}$ and $[Fe(edta)]_2O^{4-}$ species are dissociated into $[Fe^{III}L(OH)_2]$ species at higher pH. The influence of pH on the related reaction for $Fe_2O(ttha)^{2-}$ is relatively small as shown by curves A and B. When the open-chain form of $Fe^{III}_2(ttha)(H_2O)_2$ is mixed with 0.20 M H_2O_2 and the pH of the same is readjusted to 6.64 and 10.02, the respective spectra shown in C and D are obtained. The total elapsed time for pH adjustment and recording of the spectra were less than that required to obtain spectra A and B in Fig. 3 upon mixing of the μ-oxo with 0.234 M H_2O_2. A large enhancement in the absorbance above

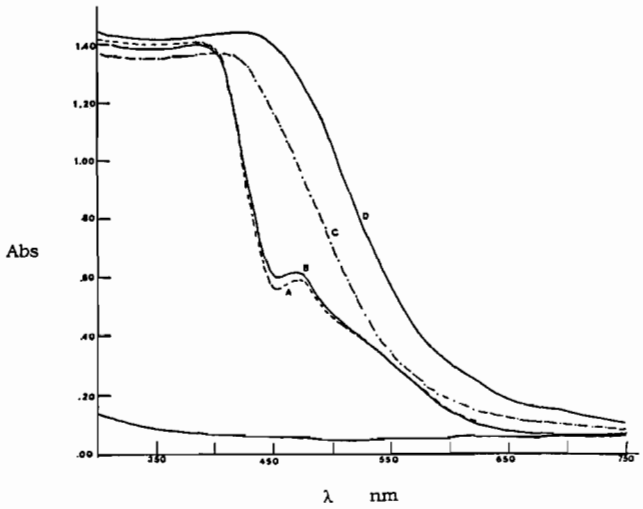

Fig. 4. Peroxo complexation by $Fe_2O(ttha)^{2-}$. $[Fe_2O(ttha)^{2-}]_i = 3.86 \times 10^{-3}$ M, 1.00 cm cell; (A) dashed curve pH 6.74; (B) same as (A) at pH = 10.07; (C) dash-dot curve, open-chain complex with $[H_2O_2]_i = 0.20$ M added and pH adjusted to 6.64; (D) same as (C) with pH adjusted to 10.02.

400 nm occurs when H_2O_2 is available for coordination. The extent of equilibrium binding of the peroxo group is sensitive to pH, increasing significantly from pH 6.64 to 10.02. Not shown in Fig. 4 are observations that below pH ~ 4 the spectra are nearly identical with or without H_2O_2 present. Open coordination positions for H_2O_2 coordination at the Fe^{III} centers are necessary to obtain this rapid change (cf. conditions of Figs. 3 and 4) and H_2O_2 must be deprotonated to enhance coordination. H_2O_2 is not efficiently bound below pH 4 but increases in the extent of coordination from pH 6.64 to 10.02.

Infrared study of the H_2O_2 oxidation products

The products of the $Fe^{II}_2(ttha)(H_2O)_2^{2-}/H_2O_2$ oxidation were isolated as Na^+ salts by the ethanol precipitation method. The amount of μ-oxo $Fe_2O(ttha)^{2-}$ was observed to decrease depending on the amount of excess H_2O_2. Data were obtained on samples precipitated immediately after the initial H_2O_2-dependent redox and substitution reactions were complete (*c.* 5 min) and prior to the interfering, slow H_2O_2-dependent changes as observed for either $Fe^{II}_2(ttha)(H_2O)_2^{2-}$ oxidized samples or with authentic $Fe_2O(ttha)^{2-}$ as described in the prior section. Representative spectra obtained at 0.06 and 0.28 M excess H_2O_2 ($Fe_2(ttha)(H_2O)_2^{2-} = 0.0275$ M) are shown in Fig. S2, A and B. The altered intensity in the 836 cm^{-1} region as a function of H_2O_2 is readily seen. The ratio of the intensity of the 836 ± 4 cm^{-1} band (authentic Fe–O–Fe stretch) [10] to the ν(COOFe) stretch at 1632 ± 4 cm^{-1} band was calculated. The baseline absorbance was estimated from the isolated solid of the open-chain

$[Fe^{III}_2(ttha)(H_2O_2)_2]$ complex. The open-chain complex was obtained by acid-induced μ-oxo bond rupture of the authentic sample [10]. The behavior of the intensity ratio $R = I_{836}/I_{1632}$ is shown in Fig. 5. The ratio R decreases linearly up to 0.40 M H_2O_2 where the intensity ratio is equal to the ratio observed for the open-chain chelate $[Fe^{III}_2(ttha)(H_2O)_2]$ (dashed line in Fig. 5). These results show that at 0.20 M excess H_2O_2 the initial reaction product mixture is only 50% μ-oxo. Another species is present which prevents complete conversion to the μ-oxo product. This species contributes negligibly to the IR intensity at 836 ± 4 cm^{-1} and accounts for the other 50% of the Fe^{III} carboxylate chromophores.

Additional samples were obtained by 0.18 M excess H_2O_2 oxidation near pH 7.0 and precipitated at 5.0 min and at 3.0 h. The band ratios at 835 versus 1635 cm^{-1} agreed with the data in Fig. 5 for both samples. This shows that the ratio of μ-oxo to peroxo products is largely controlled by the competition kinetics immediately after the oxidation step which forms the open-chain $[Fe^{III}_2(ttha)]$ derivative. This process is described in detail later in this text.

An additional feature is detectable in the expanded IR region from 500 to 1500 cm^{-1} in a comparison of the $[Fe^{III}_2(ttha)]^{n-}$ products obtained when only sufficient H_2O_2 is added to assure complete oxidation compared to the case where H_2O_2 is at a 13.6:1 ratio (0.40 M). The IR spectrum reveals an additional band at 791 cm^{-1} indicated by the arrow in Fig. 6 which appears at the same time as the band features near 836 cm^{-1} have decreased in intensity. A band at 791 cm^{-1} is also observed for the $\eta^1{:}\eta^1$ binuclear Co^{III}

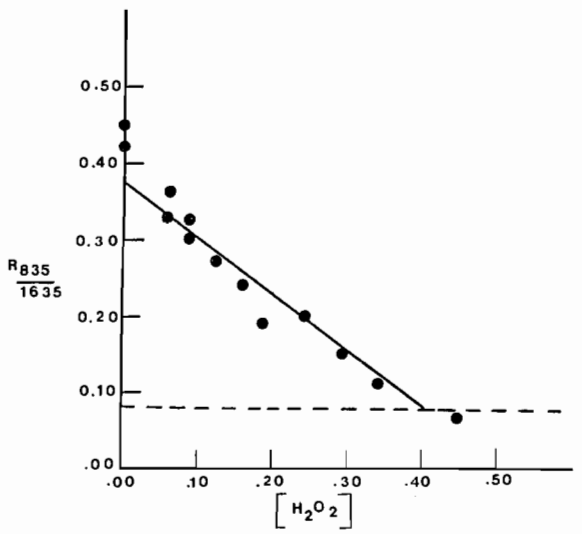

Fig. 5. Ratio of 835 cm^{-1}/1635 cm^{-1} intensities of products of the H_2O_2 oxidation of $Fe^{II}_2(ttha)(H_2O)_2^{2-}$. Dashed line shows the ratio obtained for the open-chain $Fe^{III}_2(ttha)(H_2O)_2$ solid; excess $[H_2O_2]$ varies from 0.00 to 0.45 M.

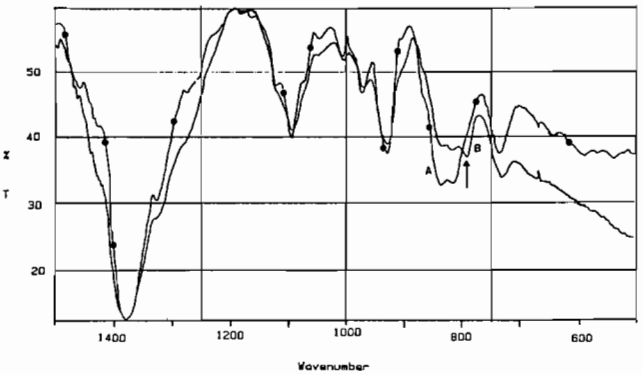

Fig. 6. IR spectra of $Fe^{III}_2(ttha)$ oxidation products as a function of H_2O_2 concentration: (A) –•–•– oxidation at $2H_2O_2$: $Fe^{II}_2(ttha)(H_2O)_2^{2-}$; (B) —— oxidation at 13.6:1.0 ratio, 0.40 M; arrow shows the appearance of the new 791 cm^{-1} band.

peroxo-bridged histidine complex, $[Co^{III}_2(O_2)(his)_4]$ [28]. Histidine provides an amine/carboxylate environment for Co^{III}. Therefore the comparison between $[Co^{III}_2(O)_2(his)_2]$ and $[Fe_2(O_2)(ttha)]^{4-}$ is probably a reasonable one from the point of view of secondary ligation around the metal centers. This suggests that the peroxo group in $[Fe_2(O_2)(ttha)]^{4-}$ is bridging the Fe^{III} centers.

It must be noted, however, that Brennan *et al.* [29] have recently observed that with diferric peroxo complexes related to HPTB and 5-Me-HXTA the ν(OO) stretch occurs between 815 and 904 cm^{-1}. The assigned diferric peroxo $\eta^1{:}\eta^1$ complexes have thus far possessed values nearer the higher end of the range, while η^2-coordinated, non-bridged species have ν(OO) stretches at the lower end [25, 29]. This is similar to the η^2 peroxo $[Fe^{III}(edta)(O_2)^{2-}$ complex which exhibits the ν(OO) band at 815 cm^{-1} [22, 23]. Therefore the IR evidence for the $[Fe^{III}_2(ttha)(O_2)]^{2-}$ complex is somewhat ambiguous in that the 791 cm^{-1} stretch can be argued as supporting either $\eta^1{:}\eta^1$ coordination based on the $[Co^{III}_2(O_2)(his)_4]$ model, or η^2 based on the $[Fe_2(HPTB)(O_2)]$ model.

There is no change in the carboxylate stretching frequency with or without H_2O_2 in the $[Fe^{III}_2(ttha)]^{n-}$ complexes: authentic $Fe_2O(ttha)^{2-}$ as the Me_2dabco^{2+} salt exhibits its ν(COOM) stretches at 1629 cm^{-1}. The solids isolated by equilibration with H_2O_2 up to 0.40 M showed no change in position or width of the stretch at 1629 cm^{-1}. There were also no shoulders in the regions for ν(COOH) or $\nu(CO_2^-)$. This establishes that all the carboxylates remain coordinated upon addition of the peroxo functionality.

An additional IR study was performed using the $[Me_2dabco][Fe_2O(ttha)]\cdot 6H_2O$ salt. An IR spectrum was obtained for the starting material. A sample was also dissolved in D_2O. The $Fe^{III}_2O(ttha)^{2-}$ complex was converted to the open-chain form by acidifying the sample with DCl. This was followed by raising the pD

with NaOD to 7 to induce reformation of Fe^{III}_2-$O(ttha)^{2-}$. The solid was precipitated by addition of *p*-dioxane, centrifuged and filtered. The solid obtained was recycled through two more DCl/NaOD sequences. This procedure was done to carry out exchange of any readily reversible H/D protonation sites. When the IR spectra were compared for the initial complex and the one taken through three D_2O exchange cycles it was observed that the spectra were identical (Fig. S3, A and B). Particular attention was given to the region near 836 cm^{-1}. If the original complex had been a hydroxy or dihydroxy bridged complex, this feature would undergo a shift by the presence of deuteriohydroxy functionalities. No change is observed; this data provides added proof that the Fe^{III} oxidation product from $Fe^{II}_2(ttha)(H_2O)_2^{2-}$ and O_2 is the μ-oxo $Fe_2O(ttha)^{2-}$ ion as reported in prior work [10].

Addition of NCS^- to $Fe_2(ttha)^{2-}$

The IR study of the peroxo addition product showed that the peroxo group adds to the $Fe_2O(ttha)^{2-}$ complex with a reduction in the intensity of the μ-oxo stretch at 836 cm^{-1}, and that no carboxylate functionalities of $ttha^{6-}$ are dissociated. An attempt was made to determine if anions such as NCS^- or Br^- could add directly to $Fe_2O(ttha)^{2-}$ without rupture of the μ-oxo bridge. Addition of 0.10 and 0.50 M NaBr or NaNCS showed minor changes in the spectrum of $Fe_2O(ttha)^{2-}$ immediately after mixing. The observed changes are attributed to high local concentrations of $X^- = Br^-$ or NCS^- which produce non-equilibrium additions of X^-. The complex reequilibrated to the same visible spectrum within 30 min. The addition of 0.50 M NCS^- was monitored as a function of pH. No change in the spectrum of $Fe_2O(ttha)^{2-}$ occurred above pH 4.80 with 0.50 M NCS^- present after equilibration. At pH 4.8 there was the permanent onset of an intense $Fe^{III} \leftarrow NCS^-$ charge transfer. A parallel study in the absence of NCS^-, but with 0.10 M NaBr present, showed that the dissociation of $Fe_2O(ttha)^{2-}$ into its open-chain form is 9% converted at pH 4.80. These results show that NCS^- does not displace a carboxylate moiety or force expansion of the coordination number at the Fe^{III} center of $Fe_2O(ttha)^{2-}$ at pH 7. There are available binding sites for NCS^- (or other ligands such as O_2^{2-}) only after the μ-oxo bridge is open.

The absence of NCS^- addition at pH 7 suggests that coordination of O_2^{2-} by an expansion of the coordination number of the Fe^{III} center without loss of the oxo unit cannot occur.

μ-Oxo ring opening and ring closure with $Fe_2O(ttha)^{2-}$

The rate of oxo-bridge rupture for $Fe_2O(ttha)^{2-}$ was followed by the proton-jump procedure, detecting the loss of the μ-oxo chromophore at 470 nm. The initial pH of a solution (9.80×10^{-3} M) was 6.68. Final pH values were 1.52, 1.60 and 2.12 under initial $[H_3O^+]$ values of 3.49×10^{-2}, 3.49×10^{-2} and 3.21×10^{-2} with oxo-bridged complex concentrations of 2.45×10^{-3}, 4.90×10^{-3} and 2.45×10^{-3} M. Consumption of H_3O^+ due to protonation of the μ-oxo bridge gave mean $[H_3O^+]$ values during the kinetic runs of 3.00×10^{-2}, 2.51×10^{-2} and 1.25×10^{-2} M with respective pseudo-first-order constants of 47.0 ± 3.5, 43.9 ± 5.2 and 24.2 ± 0.5 s^{-1}. Monomerization/dimerization pathways which involve μ-oxo bridge formation generally proceed by proton-independent and proton-assisted pathways [30, 31]. The present data also conform to the expression $k_{obs} = k_0 + k_H[H_3O^+]$ where k_0 is the rate constant for the spontaneous hydration of the oxo-bridge pathway and k_H is the proton-assisted rate constant. The data obtained at $\mu = 0.03$, $T = 25.0$ °C gave values for $k_0 = 8.3\pm1.6$ s^{-1} and $k_H = (1.9\pm0.5)\times10^3$ M^{-1} s^{-1}. The unassisted pathway (k_0) compares quite closely to the 4.0 s^{-1} valuc for thc corrcsponding monomcrization pathway for $Fe_2O(hedta)_2^{2-}$ species [30]. The rate constant for the proton-assisted rupture of $Fe_2O(ttha)^{2-}$ ($k_H = 1.19\times10^3$ M^{-1} s^{-1}) is close to the 2.51×10^3 M^{-1} s^{-1} value for the proton-assisted rupture of the dialkoxy-bridged seven-coordinate $[V(hedta\text{-}H)]_2^{2-}$ dimer which has a $[V^{III}(-(OR)]_2$ core structure [31, 32]. However, the proton-assisted rupture of $Fe_2O(ttha)^{2-}$ is 2300 times slower than the analogous dissociation rate constant (3.0×10^6 M^{-1} s^{-1}) for $Fe_2O(hedta)_2^{2-}$ [30]. This suggests that the proximity effect favors the stability of the μ-oxo bridge of $Fe_2O(ttha)^{2-}$ compared to the more facile proton-assisted dissociation of $Fe_2O(hedta)_2^{2-}$ into its monomers. It has been observed previously in the monomerization reactions of bridged binuclear complexes of both μ-oxo and dihydroxy (dialkoxy) types that the ratio of (k_H/k_0) increases as the basicity of the bridging unit increases [33]. For example, the ratio for monomerization of $(FeOH)_2^{4+}$ is 7.5×10^5 and for $Fe_2O(edta)_2^{4-}$ it is 4.2×10^8. The ratio observed in our study is 165 M^{-1}, indicative of a more highly acidic protonated oxo-bridged intermediate than with $Fe_2O(hedta)_2^{2-}$ or $Fe_2O(edta)_2^{4-}$ monomerization rc-actions. This implies greater s-character in the lone pair; which is protonated for $Fe_2O(ttha)^{2-}$ oxo-bridge opening, indicative of a greater strain in its Fe–O–Fe bond network.

The influence of the intervening ethylene bridge between the metal binding sites of $ttha^{6-}$ is of more importance for the ring-closure reaction in formation of $Fe_2O(ttha)^{2-}$ for this current study. The rate of ring closure of $Fe^{III}_2(ttha)(H_2O)_2$ at pH = 6.82 and 6.38, $\mu = 0.050$, $T = 25$ °C was determined using the pH-jump technique. A sample of $Fe_2O(ttha)^{2-}$ was obtained by O_2 oxidation of the $Fe_2(ttha)(H_2O)_2^{2-}$ complex in unbuffered media (pH = 6.86). Sample solutions were con-

verted to the open-chain form by titration with $HClO_4$ to pHs of 2.30 and 2.15. The open-chain complex solution was mixed in the stopped-flow with 2,6-lutidine/2,6-lutidinium perchlorate such that upon mixing these respective solutions the initial concentration of open-chain Fe^{III}_2(ttha) was 2.45×10^{-3} M, $\mu=0.050$ lutidinium perchlorate, pH = 6.82, $T=25$ °C or [complex] $=2.40\times10^{-3}$ M at pH = 6.38. The reappearance of the μ-oxo complex was followed at 470 nm. Two reactions are observed at pH = 6.82, one leading to a 15% increase on long times and having a pseudo-first-order rate a factor of 4 slower than the more rapid process. Only the faster process appears at pH $\leqslant$ 6.38. The more rapid process was studied in detail. On seven runs the rate constant for ring closure was found to be 0.107 ± 0.027 s^{-1} at pH = 6.82. The value of 0.128 ± 0.021 was obtained from pH = 6.38 data on 11 runs. The main source of error comes from estimating the initial A_∞ value (0.695) for the first reaction. Former dimerization studies of V^{III}(hedta) and Fe^{III}(hedta) have indicated parallel pathways for the reaction of M(hedta)(H_2O)/M(hedta)OH^- and M(hcdta)OH^-/M(hedta)OH^- partners; the aquo/hydroxy pair are the kinetically more reactive [30, 31]. Therefore it seemed logical that the first reaction below pH 6.82 represents $Fe_2O(ttha)^{2-}$ formation predominantly via reactant partners of the open-chain form with one aqua complex site and one hydroxy complex site. Based on the Fe(hedta)(H_2O) complex as a model for the terminal Fe^{III} site of the open chain, the pK_a should be *c.* 4.0. This is further supported by rate data in 0.050 M acetate and formate buffers (pHs of 4.36 and 3.36) in Fig. 7. Ring closure is accelerated up to pH 3.36 without indication of a plateau in rate. The appearance of the curve implies the pK_a of the terminal Fe^{III} site of [Fe^{III}_2(ttha)(OH_2)$_2$] must be about 2 pK units below 6.0. The limiting region at low pH near 2.0 cannot be used to locate the upper rate plateau for the diaqua complex reactivity because the thermodynamically stable form of the [Fe^{III}_2(ttha)] complex is the open-chain form. Therefore ring closure cannot be observed at the pH $\cong$ 2 limit.

The ring-closure process was also studied in sodium borate buffer ($\mu=0.050$, $T=25$ °C). The pH-jump procedure yielded a solution of final pH = 8.20 such that nearly all of the open-chain Fe^{III}_2(ttha) complex should be in the dihydroxy form. The value of k_{obs} (0.068 s^{-1}) for the overall rate of appearance and the final absorbance (0.458) are below the values at pH 6.82. The absorbance difference provides evidence that borate ion, $B(OH)_4^-$, substitutes competitively at the Fe^{III} center and then blocks ring closure. The yield of $Fe_2O(ttha)^{2-}$ is reduced to 66% in borate buffer. Additionally, the amount of $Fe_2O(ttha)^{2-}$ formed by the kinetic split between ring closure and $B(OH)_4^-$ substitution in borate buffer is further reduced on a very long time scale. A slower absorbance decrease is observed, indicative of displacement of the μ-oxo bridge with borate anions. A similar process which breaks the μ-oxo bridge of $V_2O(ttha)^{2-}$ has been reported for $H_2PO_4^-$ with an equilibrium constant form binding $H_2PO_4^-$ of $(1.7\pm0.1)\times10^3$ M^{-1} [34d]. The overall initial rate constant for appearance of the product was 0.068 ± 0.009 s^{-1} based on six runs in borate buffer. The observed constant may be corrected on the basis of the initial product distribution to include the rate of borate complex formation at 0.05 M (1.6 M^{-1} s^{-1}) and the intrinsic rate of μ-oxo formation under these conditions of 0.027 s^{-1}. Additionally, the rate of ring closure at pH near 7.0 ($k=0.107\pm0.027$ s^{-1}) is in excellent with the value of 0.1 s^{-1} estimated from the kinetically determined product distribution established by the IR analysis of the products*.

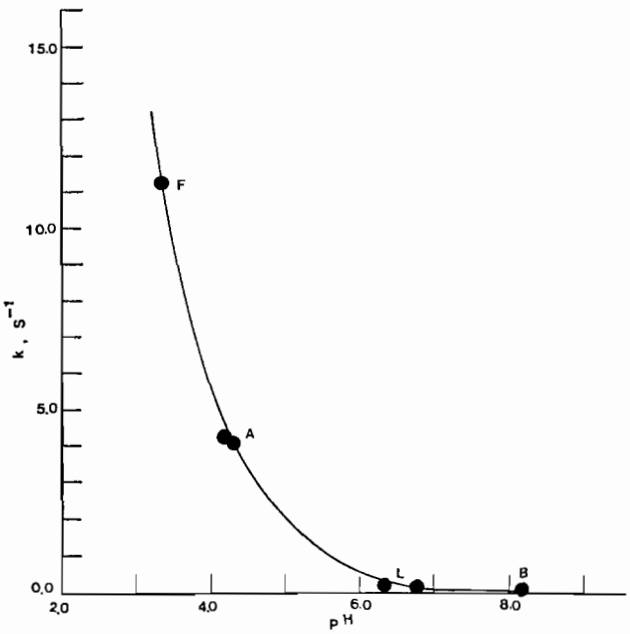

Fig. 7. Rate of appearance of the 470 nm absorbance during the μ-oxo $Fe_2O(ttha)^{2-}$ formation in buffers. $T=25.0$ °C; $\mu=0.050$; F = formate, A = acetate, L = lutidine, B = borate.

The data in Fig. 7 were fit to the following equilibria and kinctic processes for the ring-closure reaction

*An estimate of 0.1 s^{-1} for the ring-closure rate can also be determined from the competition between ring closure and peroxo complex formation as determined by the isolated products in the IR study. This estimate requires an estimated rate of H_2O_2 substitution on an Fe^{III} site of Fe^{III}_2(ttha)(H_2O)$_2$ of between 2.5 and 25 M^{-1} s^{-1} which is based on the 250 M^{-1} s^{-1} for H_2O_2 substitution on Fe(edta)(H_2O)$^-$ [34a] reduced by a factor of 10 to 100 for the lower coordination number of an Fe^{III}_2(ttha)(H_2O)$_2$ site.

$$H_2O\text{—}Fe\text{⁓}FeOH_2 \underset{}{\overset{K_{a1}}{\rightleftharpoons}} H_2O\text{—}Fe\text{⁓}FeOH + H_3O^+ \quad (10)$$
(A) (B)

$$H_2O\text{—}Fe\text{⁓}FeOH_2 \overset{K_{a2}}{\rightleftharpoons} HO\text{—}Fe\text{⁓}Fe\text{—}OH + H_3O^+ \quad (11)$$
(B) (C)

$$A \xrightarrow{k_1} Fe\text{⁓}O\text{⁓}Fe + 2H_3O^+ \quad (12)$$

$$B \xrightarrow{k_2} Fe\text{⁓}O\text{⁓}Fe + H_3O^+ \quad (13)$$

$$C \xrightarrow{k_3} Fe\text{⁓}O\text{⁓}Fe + H_2O \quad (14)$$

The distribution of species A, B and C was calculated from evaluation of α values in the manner of a diprotic acid dissociation [35] using estimates of $K_{a2} = 1.0 \times 10^{-4}$ M^{-1} derived from the titration behavior in Fig. 7 ($pK_{a2} = 4.0$) and the knowledge that K_{a1} will be a statistical factor of 2 larger ($pK_{a1} \cong 3.7$). The derived constants were found to require a significant contribution from the reactivity of the diaqua species (A) in order to obtain a real solution for k_1, k_2 and k_3*. The values for the respective constants were $k_1 = 12.0$, $k_2 = 11.6$ and $k_3 = 0.11$ s^{-1}. The ratio of the rate constants (k_2/k_3) compares the reactivity of the binuclear complex with one aqua and one hydroxy site (B) with the dihydroxy complex (C). The value of 105 obtained from the kinetic fit is in good agreement with the ratios of 67 and 33 found for these pathways in the formation of $Fe_2O(hedta)_2^{2-}$ and $Fe_2O(edta)_2^{4-}$, respectively [34]. The unusual case is the relative high reactivity of the diaqua complex (A) which is found to have much lower reactivity in the formation of a μ-oxo bridge when separate mononuclear species combine in their respective dimer [30, 31, 36]. The values obtained for k_1 (12.0 s^{-1}) and k_2 (11.6 s^{-1}) are the same within experimental error, as necessitated by the estimation on K_{a1} and K_{a2}. The reason for the higher reactivity via the diaqua pathway in the μ-oxo formation with $Fe^{III}_2(tha)(H_2O)_2$ would seem to reside in the proximity advantage which cannot be matched for monomeric aqua species combining to form a μ-oxo dimer. The latter process requires reorganization of two independent solvent cages while the $Fe^{III}_2(tha)(H_2O)_2$ bridging reaction proceeds within one large solvent perturbed environment. If prior association of the terminal sites of the aqua/aqua and aqua/hydroxy pairs of reactants occurs, one can envision relatively similar transition states for removal of two and one protons, respectively, with formation of an oxo-bridge via displacement of a water molecule

*The rate law for parallel pathways was assumed:

$$\frac{d[dimer]}{dt} = \frac{dA_{470}}{dt} = (k_1\alpha_0 + k_2\alpha_1 + k_3\alpha_2)[binuclear]_{tot};$$

α_0 = fraction of A, α_1 = fraction of B, α_2 = fraction of C.

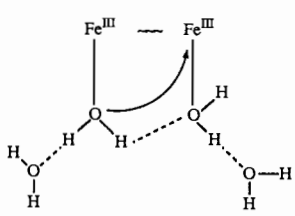

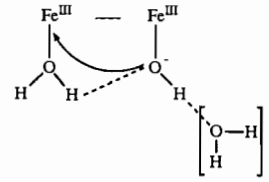

Molecular models of the open-chain $Fe^{III}_2(tha)(H_2O)_2$ complex show that a near placement of the coordinated waters or water/hydroxy ligand pair, with an intervening μ-H_3O_2 H-bonded network to stabilize the required orientations, is readily achieved. Evidence for the μ-$H_3O_2^-$ bridging unit has been obtained from Cr(III), Mo(III) and W(III) clusters [37, 38] and has been proposed to facilitate the $Fe^{II/III}$ electron transfer [39]. However, when two anion ends of the Fe^{III}_2-$(tha)(OH)_2^-$ complex attempt to combine in the k_3 pathway for species C, an electrostatic reduction in rate constant, comparable to the combination of $Fe(hedta)OH^-$ anions, is observed.

H_2O_2 substitution on open-chain $[Fe^{III}_2(tha)]$

A 4.80×10^{-3} M $Fe_2(tha)(H_2O)_2$ solution was prepared at pH = 2.15 by acidification of the μ-oxo complex. This solution was mixed by the stopped-flow method with 2,6-lutidine/2,6-lutidinium buffers containing 0.100, 0.200 and 0.400 M H_2O_2 after the stopped-flow dilution. The initial concentration of the open-chain complex was 2.40×10^{-3} M at pH = 6.38. At the higher H_2O_2 concentrations (0.200 and 0.400 M) a slower second reaction was observed. The slower reaction occurred with an absorbance decrease after a faster process yielding an increasing absorbance (Table 1).

The data for reaction (1) shows that the final absorbance for reaction (1) increases with the amount of H_2O_2 in the solution. The change in absorbance for reaction (2) was at least 1.5 times as great (0.121 units) at 0.400 M as at 0.200 M (0.082). The estimate of the difference in ΔA is complicated by a receding A_∞ in reaction (1). It is consistent, however, with results

TABLE 1. Addition of H_2O_2 to $[Fe^{III}_2(tha)]$ at pH 6.38[a]

$[H_2O_2]$ (M)	Reaction	A_∞	k (s^{-1})	No. runs
0.00	RC	0.639	0.128 ± 0.021	11
0.100	1	0.734	1.172 ± 0.078	12
0.200	1	0.830	1.661 ± 0.140	6
0.200	2	0.748	0.144 ± 0.014	4
0.400	1	0.946	2.480 ± 0.127	9
0.400	2	0.825	0.199 ± 0.025	5

[a]μ = 0.05 lutidine/lutidinium buffer, $[Fe_2(tha)]_i = 2.40 \times 10^{-3}$ M, T = 25 °C, RC = ring-closure reaction forming $Fe_2O(tha)^{2-}$ only.

predicted by the IR studies that twice as much of the peroxo product forms at 0.400 M compared to 0.200 M. Within experimental error the rate constant for the second process is independent of $[H_2O_2]$. However, the initial absorbance change is first-order in $[H_2O_2]$ (Fig. S4). Treatment of the kinetic data by least-squares gives a slope of 4.32 ± 0.20 M^{-1} s^{-1} and an intercept of 0.763 ± 0.052 s^{-1}. The slope (rate constant for the H_2O_2-dependent process) falls within the range of 2.5 to 25 M^{-1} s^{-1} as estimated for the addition of H_2O_2 to a hydroxy moiety of the open-chain $[Fe_2(ttha)]$ species. The slower process which yields a decreasing absorbance (reaction (2)) cannot be the addition of H_2O_2 to $Fe_2O(ttha)^{2-}$ as this reaction occurs on the hours time scale ($t_{1/2} \cong 1.6$ h) as shown in a prior section. The rate constant of *c.* 0.13 ± 0.03 s^{-1} for the second process is similar to the value for ring closure to form the μ-oxo complex, (0.128 ± 0.021) s^{-1}. However, the pathway forming the μ-oxo product will operate competitively with H_2O_2 substitution. Since the latter is the faster pseudo-first-order process ($k = 0.432$, 0.864 and 1.73 s^{-1} at 0.100, 0.200 and 0.400 M H_2O_2, respectively) none of the open-chain complex would be left unbound by H_2O_2 or as the initial μ-oxo product at the conclusion of the first increasing absorbance change. Additionally, the total decrease in absorbance of the slower process is proportional to the amount of the first peroxo species formed during the kinetic competition between μ-oxo ring closure and H_2O_2 substitution. Therefore we conclude that the second slower process at high $[H_2O_2]$ represents the detection of a rearrangement in the coordination mode of the peroxo complex which is formed during the substitution of H_2O_2. Since it is known that $Fe^{III}(edta)(O_2)^{3-}$ is formed as the η^2 complex [21, 23], it seems that our data is best accommodated by the initial addition of H_2O_2 at a hydroxy site of the open-chain $[Fe^{III}_2(ttha)]$. The slower rearrangement appears to have nearly the same kinetic restraints as the μ-oxo ring-closure reaction via the dihydroxy partners. It is logical to assign the rearrangement process to the formation of a bridged $\eta^1{:}\eta^1$ complex.

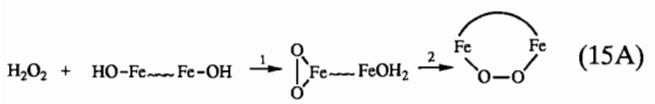

(15A)

An alternative possibility must be acknowledged in consideration of the recent report of Brennan *et al.* [29] in regard to diferric peroxo complexes favoring η^2 coordination for species having the ν(OO) stretch near 815 cm^{-1}. The two steps detected by the stopped-flow method would then indicate a switch between η^1 coordination, obtained in the first peroxide-dependent step, to η^2 coordination in the final product, e.g. sequence (15B) where parallel reactions occur at all available Fe^{III} sites simultaneously.

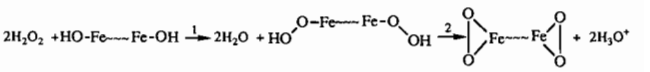

(15B)

It is most unlikely, however, that step 2 would yield a decreasing absorbance given the more negative charges of the η^2 peroxo complexes. An η^1-bound peroxo species is shown in the next section to have a much lesser absorbance than η^2-bound peroxo groups at Fe^{III} sites of Fe^{III}(hedta). Furthermore, the species found in step 1 of (15B) is found to be unstable when H is replaced with $(CH_3)_3C-$ as described in a later section. These facts favor (15A) as the correct sequence, supporting $\eta^1{:}\eta^1$ bridging by the peroxo ligand.

The intercept value of Fig. S4 implies that there is an additional process which contributes to the first A_∞ value that is not accounted for by the simple sequence (15A or 15B). The ring-closure competitive process contributes 0.128 ± 0.021 s^{-1}, but this does not account for all of the observed 0.76 s^{-1}. The residual 0.635 s^{-1} must be an H_2O_2-independent process which is not present when the open-chain complex is mixed with the buffer alone. The most probable process for this pathway would be the substitution of H_2O_2 for the aqua ligand at an $[Fe_2(ttha)]$ terminal site with rupture of the Fe^{III}–aqua bond being the rate limiting event, e.g. eqn. (16), via an interchange mechanism.

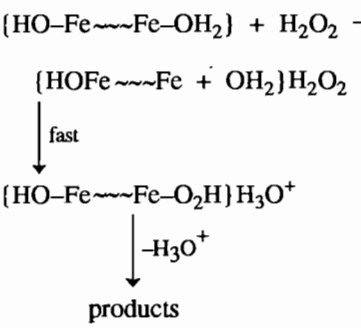

(16)

The possible substitution of H_2O_2 in acetate buffer $\mu = 0.050$, pH = 4.36 was studied with and without 0.400 M H_2O_2. The apparent rate constant of reaction of the open-chain form at pH 4.36 was 4.04 ± 0.16 s^{-1} in the absence of H_2O_2 and 3.95 ± 0.21 s^{-1} with 0.400 M H_2O_2 present. This data infers that coordination of H_2O_2 does not take place at pH 4.36, but rather only the ring-closure path occurs, a result in concert with the evidence presented concerning Fig. 4 in a prior section.

Peroxo complexation of Fe^{III}(hedta)(H_2O)

The normal instability of Fe^{III}–peroxo complexes with pac ligands [15, 16] and the unusual spectra presented in Fig. 4 prompted an investigation of the behavior of Fe^{III}(hedta)(H_2O) toward coordination of H_2O_2. The $hedta^{3-}$ ligand set is a good approximation to one of

the two binding sites for binuclear complexes of $ttha^{6-}$. Thus the $Fe^{III}(hedta)(H_2O)$ site represents one-half of $Fe^{III}_2(ttha)(H_2O)_2^{2-}$. Equilibria for the formation of $Fe_2O(hedta)_2^{2-}$ have been thoroughly studied [34]. Important equilibria are presented in eqns. (17)–(19). The μ-oxo binuclear complex is favored in the pH

$$Fe(hedta)(H_2O) \rightleftharpoons Fe(hedta)(OH)^- + H_3O^+ \quad (17)$$

$$2Fe(hedta)(OH)^- \rightleftharpoons Fe_2O(hedta)_2^{2-} + H_2O \quad (18)$$

$$Fe(hedta)(OH)^- + OH^- \rightleftharpoons Fe(hedta)(OH)_2^{2-} \quad (19)$$

range of 4.50 to 9.00. The brownish-orange $Fe_2O(hedta)_2^{2-}$ species forms with increasing absorbance in the region from 450 to 600 nm throughout this range. The binuclear complex has the characteristic bands at 470 nm and a shoulder at 550 nm as described previously [10]. In the pH range of 9 to 11 the dihydroxy complex forms (eqn. (19)), and the absorbance decreases. The solution color reverts to a pale yellow. This is shown in Fig. 8, spectra A–C. When H_2O_2 is present at pH $\geq$ 9.70, the absorbance is not below that of the $Fe_2O(hedta)_2^{2-}$ complex due to the normal pH-induced shift of equilibria (17)–(19), but rather a higher absorbing species is obtained as seen in A–C. The solution color is a distinct golden-brown color, different from either $Fe(hedta)(OH)_2^{2-}$ or $Fe_2O(hedta)_2^{2-}$. Additionally when the pH of a solution of $[Fe(hedta)(H_2O)] = 4.85 \times 10^{-3}$ M is adjusted upward from 4 to 9 in the presence of $[H_2O_2] \geq 0.017$ M the solution remains a light yellow color, not the brownish-orange of the solution in response to equilibria (17) and (18) as in the absence of H_2O_2. When $(CH_3)_3COOH$ (0.53 M) is used in place of H_2O_2 the spectrum shows no absorbance equal to the spectra in the absence of H_2O_2 or $(CH_3)_3COOH$. All absorbance curves reside below that of the equilibrium amounts of $Fe(hedta)(H_2O)/Fe(hedta)(OH)^-/Fe_2O(hedta)^{2-}/Fe(hedta)(OH)_2^{2-}$ at every pH value from 4.16 to 11.54. It is significant that the golden-brown color of the Fe(hedta) solution with H_2O_2 above pH 10 is not observed when $(CH_3)_3COOH$ is present, but both H_2O_2 and $(CH_3)_3COOH$ retard the formation of $Fe_2O(hedta)^{2-}$ in the pH range of 4 to 8. These observations are consistent with the coordination changes shown in Scheme 2. It was additionally observed that Fe(hedta) with H_2O_2 above pH 10 slowly evolves O_2 and will revert to $Fe_2O(hedta)_2^{2-}$ after 20 h. With the additional information that $Fe^{III}(edta)^-$ forms the well-known η^2 peroxo complex, $[Fe(edta)(O_2)]^{3-}$, which exhibits its characteristic purple color only in the range of pH $\geq$ 9.5 [23], oxygen evolution and hydroxylation pathways in basic H_2O_2 solutions [20], it would appear most likely that the golden-brown $Fe(hedta)(O_2)^{2-}$ complex formed in the same pH range is also an η^2-bound complex. A conformation of the η^2 bonding mode was made by preparation of $[Fe^{III}(hedta)(H_2O)]$ by the autoxidation of $Fe^{II}(hedta)(H_2O)^-$ in solution.

The resultant $Fe^{III}(hedta)$ product was split into three identical samples. These were adjusted to pH 7, where the binuclear oxo-bridged form is stable; pH 10.30 where significant amounts of $[Fe(hedta)(OH)_2]^-$ exists in equilibrium with $Fe_2O(hedta)_2^{2-}$; and the third sample was adjusted to pH 10.30 in the presence of 0.20 M H_2O_2. Each of the three samples was concentrated by rotary evaporation and precipitation was induced

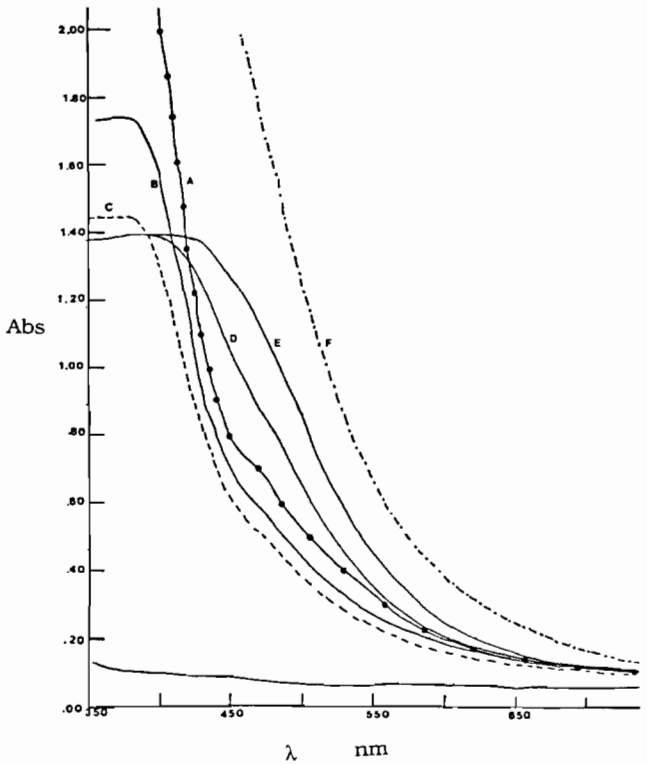

Fig. 8. Peroxo complexation by $Fe^{III}(hedta)$. $[Fe^{III}(hedta)]_i = 4.85 \times 10^{-3}$ M; 1.00 cm cell; (A) $Fe^{III}(hedta)$ only at pH = 7.66; (B) same as (A) at pH = 9.58; C same as (A) at 10.07; (D) H_2O_2 added, $[H_2O_2]_i = 1.70 \times 10^{-2}$ M, pH = 9.70; (E) $[H_2O_2]_i = 8.50 \times 10^{-2}$ M, pH = 11.70. Solutions (E) and (F) are metastable and evolve O_2.

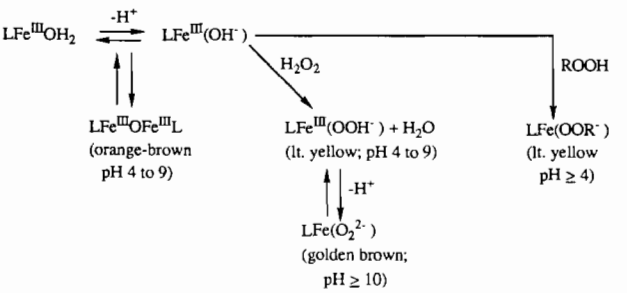

Scheme 2. Reactions of H_2O_2 or ROOH with $Fe^{III}(hedta)(H_2O) = (LFe^{III}OH_2)$.

by the addition of ethanol. The solid products as sodium salts were rinsed with absolute ethanol and dried at 30 °C in a vacuum oven. IR spectra were obtained on each of the solids. The two samples without H_2O_2 gave the anticipated spectra in accordance with the literature. A band at 833 cm^{-1} assigned to the asymmetric μ-oxo stretch was clearly observed. The sample treated with H_2O_2 at pH 10.30 showed a much diminished band at 833 cm^{-1} and the presence of a stronger band at 810 cm^{-1} (Fig. 9). This is coincident with the position for the ν(O–O) vibration reported for the η^2-bound peroxo complex of $edta^{4-}$, $[Fe(edta)(O_2)]^{3-}$ as reported by Loehr and co-workers [21, 22]. Thus the golden-brown solution yields an analogous $[Fe^{III}(hedta)(O_2)]^{2-}$ complex whose properties are those reported for η^2 coordination in a related complex. We conclude the peroxo complex of Fe^{III}(hedta) is also bound in the η^2 mode.

The similarity of H_2O_2 and $(CH_3)_3COOH$ to inhibit μ-oxo dimer formation in the pH range of 4–9 and to produce the same light yellow chromophore with Fe(hedta) implies that the HO_2^- or $(CH_3)_3COO^-$ anions are coordinated in this range, preventing $Fe_2O(hedta)_2^{2-}$ formation. The bonding mode of $(CH_3)_3COO^-$ is less certain as numerous η^2-alkyl peroxo complexes are reported in catalytic systems [3]. Hindrance of the t-butyl group may favor the η^1 attachment for $(CH_3)_3COO^-$. The absence of a charge transfer band above 400 nm is explained by the less polarizable electron clouds for the HO_2^- and $(CH_3)_3COO^-$ anions compared to O_2^{2-} which provides this LMCT transition for both $[Fe(edta)(O_2)]^{3-}$ (λ_{max}=528) and $[Fe(hedta)(O_2)]^{2-}$. The important aspect of the latter case is that the band position is at higher energy (<500 nm) than is normally reported for peroxo complexes of Fe^{III} [25, 29]. This result is in concert with the behavior of H_2O_2 addition to $Fe^{III}(ttha)(H_2O)_2$ (Fig. 4) where a band below 500 nm is also observed upon coordination of H_2O_2.

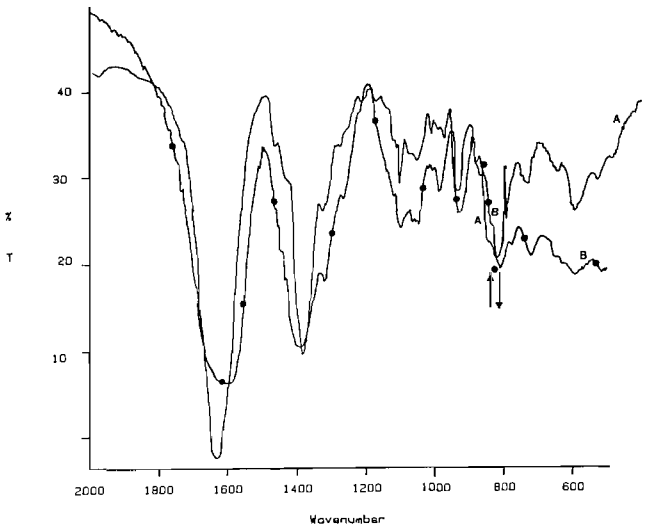

Fig. 9. Comparison of IR spectra of Fe^{III}(hedta) species isolated at pH 10.30. —— (A) $Fe^{III}(hedta)(H_2O)$ adjusted to pH 10.30 alone. –·– (B) same as (A) adjusted with 0.20 M H_2O_2 present.

Conclusions

The oxidation mechanisms of $Fe^{II}_2(ttha)(H_2O)_2^{2-}$ by O_2 and H_2O_2 are clearly different. When O_2 is the oxidant, the product is almost quantitatively $Fe_2O(ttha)^{2-}$. When H_2O_2 is the oxidant a significant amount (20%) of the Fe^{III} product is a tetranuclear $[Fe_4(O)_2(ttha)]^{4-}$ complex in addition to $Fe_2O(ttha)^{2-}$. A small amount of demetallated material which includes $FeCl_4^-$ and $Fe^{III}(tthaH)^{2-}$ was also detected during H_2O_2 oxidation. The oxidation by H_2O_2 occurs with a small suppression (*c.* 6.8%) in the presence of t-butanol, a scavenger for HO·, but t-butanol has no net effect on the O_2 oxidation of $Fe^{II}_2(ttha)(H_2O)_2^{2-}$. The amount of suppression of overall oxidation by 0.10 M t-butanol is within a few percent of the suppression observed by Rush and Koppenol in the H_2O_2 oxidation of $Fe^{II}(edta)^{2-}$ [18]. A sequential $1e^-$ oxidation of $Fe^{II}_2(ttha)(H_2O)_2^{2-}$ by H_2O_2 is ruled out by the minor extent of HO· production during the oxidation process as detected by the t-butanol method.

Rush and Koppenol have observed that the cross-reaction between a ferryl complex $[(Fe^{IV}O)edta)]^{2-}$ and $Fe^{II}(edta)^{2-}$ was a facile reaction, accounting for about 80% of redox events when $[Fe^{II}]_{tot}$:$[H_2O_2] \geq 0.1:1$ [18]. A modification of the overall reaction scheme given in eqns. (2)–(8) is necessary to explain the data of our report on the $Fe^{II}_2(ttha)(H_2O)_2^{2-}/H_2O_2$ reaction. The open-chain $Fe_2(ttha)(H_2O)_2^{2-}$ complex will be represented as $Fe^{II} \sim \sim \sim Fe^{II}$ to emphasize the separate Fe^{II}(pac) binding sites in the complex. Initiation by a $2e^-$ oxidation occurs, analogous to eqn. (2), via eqn. (20). The ferryl site is indicated by $\sim \sim \sim Fe^{IV}O$.

$$Fe^{II} \sim\sim Fe^{II} + H_2O_2 \longrightarrow Fe^{II} \sim\sim Fe^{IV}O + H_2O \quad (20)$$

$$Fe^{II} \sim\sim Fe^{IV}O \xrightarrow{1SET} Fe^{III}\overset{O}{\diagdown\diagup}Fe^{III} \quad (21)$$

$$Fe^{II} \sim\sim Fe^{IV}O \xrightarrow{OSET,\ H^+} Fe^{III} \sim\sim Fe^{III}\text{–}OH \quad (22)$$

$$Fe^{III} \sim\sim Fe^{III}OH \xrightarrow{RC} Fe^{III}\overset{O}{\diagdown\diagup}Fe^{III} \quad (23)$$

$$Fe^{II} \sim\sim Fe^{IV}O + H_2O_2 \longrightarrow Fe^{II} \sim\sim Fe\overset{O}{\diagdown\diagup}\overset{H}{O\text{–}O} \quad (24)$$

$$Fe^{II} \sim\sim Fe\overset{O}{\diagdown\diagup}\overset{H}{O\text{–}O} \longrightarrow Fe^{II} \sim\sim Fe^{III}(O_2H^-) + HO\cdot \quad (25)$$

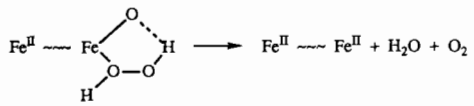

(26)

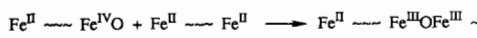

(27)

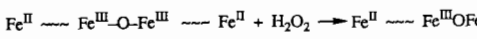

(28)

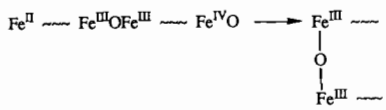

(29)

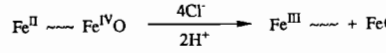

(30)

In this sequence the main pathways involve reactions (20), (21), (24), (26) and (27)–(29). Initial formation of an Fe^{IV}(pac) ferryl site is followed by reduction of the $Fe^{IV}O$(pac) chromophore. This may occur by either inner-sphere electron transfer (eqn. (21)) in which the reducing Fe^{II} site swings close to the $Fe^{IV}O$ site and forms the μ-oxo bridge, or the sequence can be a two-step process of outer-sphere electron transfer between sites of close proximity (eqn. (22)) followed by ring closure through hydrolytic polymerization (eqn. (23)). The ring-closure process is in the stopped-flow time scale and was studied separately as described in the relevant section of this text. The channels (20)–(23) represent about 80% of the redox steps generating an Fe^{III} product as identified by the ion exchange studies. The tetranuclear product (4^- anion) which was identified as another 20% (approximate) is readily accommodated by the processes in eqns. (27)–(29). These represent inner-sphere electron transfer between one $Fe^{IV}O$(pac) and one Fe^{II}(pac) site. However, the inner-sphere reaction partner is obtained from another $Fe^{II}_2(ttha)(H_2O)_2^{2-}$ reactant. The approach of these species in eqn. (27) is no worse electrostatically than the same process for $Fe^{IV}O(edta)^{2-}$ and $Fe^{II}(edta)^{2-}$ in the study of Koppenol and co-workers [18, 19]. Therefore it is of no real surprise that cross-linking can occur in the $Fe^{II}_2(ttha)(H_2O)_2^{2-}$ reaction with H_2O_2. Models show that the tetranuclear open-chain intermediate formed in eqn. (28) and consumed in eqn. (29) come together with relative ease to form the cross-linked tetranuclear complex, isolated with 1.88 M Na_2SO_4 by ion exchange.

The channel which causes the stoichiometry of H_2O_2 consumed by oxidation to become greater than one is the reduction pathway, eqns. (24)–(26). The reduction of high valent metal oxo groups by H_2O_2 is well known. Koppenol estimates the reduction potential of $Fe^{IV}(edta)^{2-}$ as 1.00 V at pH 7 [18]. Therefore the overall reduction by H_2O_2 in steps (24) and (26) is favorable. This pathway consumes 42% of H_2O_2. The pathway leading to $HO^{\cdot}$ is a minor one, yielding about 6% of redox events upon reaction of isolated $Fe^{IV}O$(pac) sites with H_2O_2. We have envisioned the placement of the incoming H_2O_2 moiety in a cyclic arrangement as described by Mimoun for the substitution of H_2O_2 displacing a metal oxo group [3]. Electron arrangement within this moiety can lead to either O_2 evolution (eqn. (26)) or less efficiently to form $HO^{\cdot}$ which escapes the cage (eqn. (25)) to leave behind a peroxy anion at the Fe^{III} site. We have not shown all the possible pathways which result from reduction of $HO^{\cdot}$ by the Fe^{II} pool or atom abstraction process (eqn. (7)) because the contributions of such paths are minor. It was also noted in the ion exchange experiments that higher-order cross-polymers were absent. Thus it appears that statistically eqn. (29) consumates all of the steps leading to the tetramer level. This is reasonable given that pathways leading to $Fe_2O(ttha)^{2-}$ (eqns. (21)–(23)) represent 80% of the processes leading to Fe^{III} products.

Pathway (24)–(26) is very efficient at high $[H_2O_2]$. This forces the system to cycle such that the open-chain form via pathway (22) is generated in abundance as all $Fe^{IV}O$ reactions with Fe^{II} by inner-sphere routes are swamped out by competition through eqn. (26).

The proposed mechanism for further addition of H_2O_2 in competition with ring closure to produce $Fe_2O(ttha)^{2-}$ is shown in Scheme 3 (near pH 7). The rate constants have been measured by stopped-flow methods. The observed second-order rate constant of 4.32 M^{-1} cm^{-1} is compatible with the known rate of addition of H_2O_2 on $Fe(edta)^-$ as described in a prior section of this paper.

Both H_2O_2 and $(CH_3)_3COOH$ inhibit μ-oxo formation of $Fe_2O(hedta)_2^{2-}$ from mononuclear $Fe(hedta)(H_2O)$ by shifting of equilibria in favor of the respective monomeric $Fe^{III}(hedta)(OOR)^-$ complexes (R = H and $(CH_3)_3C$). But $(CH_3)_3COOH$ was not observed to inhibit

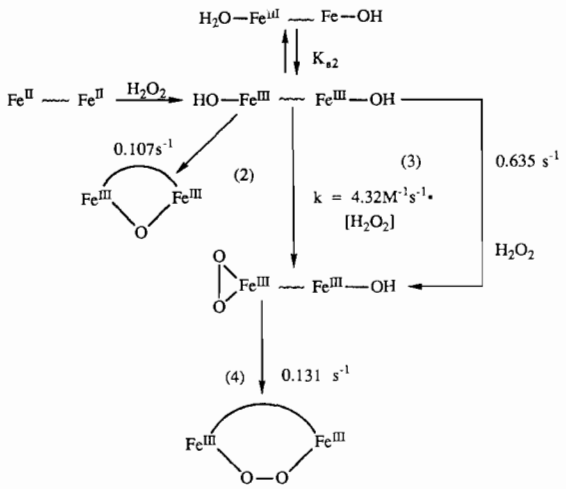

Scheme 3.

formation of $Fe_2O(ttha)^{2-}$. H_2O_2 on the other hand promotes the formation of a new species as shown by Fig. 4. Therefore we infer that the peroxo entity is an $\eta^1{:}\eta^1$ complex as shown in Scheme 2 since this arrangement would be sterically hindered for coordination of $(CH_3)_3COO^-$ in a bridging manner, but accessible for O_2^{2-} as a bridging ligand. The issue of whether a diferric peroxo complex of $\eta^1{:}\eta^1$ coordination is compatible with a ν(OO) band at 791 cm^{-1} remains a question which will require an additional resonance Raman and isotopic labelling study in future work.

Supplementary material

Additional figures mentioned in the text as Figs. S1–S4 are available from the authors on request.

Acknowledgement

We gratefully acknowledge support of this work under National Science Foundation grant CHE-8417751.

References

1 (a) A. E. Martell and D. T. Sawyer (eds.), *Oxygen Complexes and Oxygen Activation by Metal Complexes,* Plenum, New York, 1988; (b) T. G. Spiro (ed.), *Metal Ion Activation of Dioxygen, Metal Ions in Biology Series,* Vol. 2, Wiley–Interscience, New York, 1980; (c) O. Hayaishi (ed.), *Molecular Mechanisms of Oxygen Activation,* Academic Press, New York, 1974; (d) L. I. Simandi (ed.), *Dioxygen Activation and Homogeneous Catalytic Oxidation,* Elsevier, Amsterdam, 1991; (e) J. P. Collman, P. D. Hampton and J. I. Brauman, *J. Am. Chem. Soc., 112* (1990) 2977; (f) *112* (1990) 2986; (g) A. J. Castellino and T. C. Bruice, *J. Am. Chem. Soc., 110* (1988) 158; (h) T. G. Traylor, Y. Iamamoto and T. Nakano, *J. Am. Chem. Soc., 108* (1986) 3529; (i) J. T. Groves, G. A. McClusky, R. E. White and J. J. Coon, *J. Biochem. Biophys. Res. Commun., 81* (1978) 154; (j) J. T. Groves and Y. J. Watanabe, *J. Am. Chem. Soc., 108* (1986) 7834; (k) J. S. Valentine, J. N. Burstyn and C. D. Margeum, in A. E. Martell and D. T. Sawyer (eds.), *Oxygen Complexes and Oxygen Activation by Transition Metals,* Plenum, New York, 1988, pp. 175–187; (l) D. T. Sawyer, pp. 129–148.

2 (a) P. N. Balasubramamian and T. C. Bruice, *Proc. Natl. Acad. Sci. U.S.A., 84* (1987) 1734; (b) P. C. Wilkins and R. G. Wilkins, *Coord. Chem. Rev., 79* (1987) 195.

3 H. Mimoun, in G. Wilkinson, R. D. Gillard and J. A. McLeverty (eds.), *Comprehensive Coordination Chemistry,* Vol. 6, Pergamon, New York, 1987, pp. 317–410.

4 (a) G. Minotti and S. D. Aust, *Chem. Phys. Lipids, 44* (1987) 191; (b) B. Halliwell and J. M. C. Gutteridge, *Arch. Biochem. Biophys., 246* (1986) 501; (c) J. Fee, in T. G. Spiro (ed.), *Metal Ion Activation of Dioxygen,* Wiley–Interscience, New York, 1980, pp. 209–237.

5 P. B. Balasubramamian, and T. C. Bruice, *J. Am. Chem. Soc., 108* (1986) 5495.

6 S. Rakhal and H. W. Richter, *J. Am. Chem. Soc., 110* (1988) 3126.

7 (a) C. Bull, G. J. McClune and J. A. Fee, *J. Am. Chem. Soc., 105* (1983) 5290; (b) G. J. McClune, J. A. Fee, G. A. McCluskey and J. T. Groves, *J. Am. Chem. Soc., 99* (1977) 5220.

8 E. N. Rizkalla, O. H. El-Shafey and N. M. Grundy, *Inorg. Chim. Acta, 57* (1982) 199.

9 (a) J. D. Rush and W. H. Koppenol, *J. Am. Chem. Soc., 110* (1988) 4957; (b) K. C. Francis, D. Cummins and J. Oakes, *J. Chem. Soc., Dalton Trans.,* (1985) 493.

10 R. E. Shepherd, T. K. Myser and M. G. Elliott, *Inorg. Chem., 27* (1988) 916.

11 V. Zang and R. van Eldik, *Inorg. Chem., 29* (1990) 1705.

12 Y. Kurimura, R. Ochiai and N. Matsuura, *Bull. Chem. Soc. Jpn., 41* (1968) 2234.

13 (a) S. O. Travin and Y. I. Skurlatov, *Russ. J. Phys. Chem. (Engl. Transl.), 55* (1981) 815; (b) A. P. Purmal, Y. I. Skurlatov and S. O. Travin, *Bull. Acad. Sci. USSR, Div. Chem. Sci. (Engl. Transl.), 29* (1980) 315.

14 (a) Y. Nishida, M. Takeuchi, H. Shimo and S. Kida, *Inorg. Chim. Acta, 96* (1984) 115; (b) P. Murch, F. C. Bradley and L. Que, *J. Am. Chem. Soc., 108* (1986) 5027.

15 E. C. Niederhoffer, J. H. Timmons and A. E. Martell, *Chem. Rev.,* (1984) 137.

16 E.-I. Ochiai, *Inorg. Nucl. Chem. Lett., 10* (1974) 453.

17 D. T. Sawyer, S. Leshing, H.-C. Tung and A. Sobkowski, in L. Simandi (ed.), *Dioxygen Activation and Homogeneous Catalytic Oxidation,* Elsevier, Amsterdam, 1991, pp. 285–295.

18 (a) J. D. Rush and W. H. Koppenol, *J. Inorg. Biochem., 29* (1987) 199; (b) *J. Biol. Chem., 261* (1986) 6730.

19 J. D. Rush, Z. Maskos and W. H. Koppenol, in L. Packer and A. N. Glazer (eds.), *Methods in Enzymology, Vol. 186: Oxygen Radicals in Biological Systems, Part B (Oxygen Radicals and Antioxidants),* Academic Press, San Diego, 1990, pp. 148–156.

20 C. Walling, *Acc. Chem. Res., 8* (1975) 125.

21 (a) S. Ahmad, J. D. McCallum, A. K. Shiemke, E. H. Appelman, T. M. Loehr and J. Sanders-Loehr, *J. Inorg. Chem., 27* (1988) 2230; (b) F. A. Cotton and G. Wilkinson, *Advanced Inorganic Chemistry,* Wiley–Interscience, New York, 5th edn., 1988, pp. 468–470.

22 T. M. Loehr, in A. E. Martell and D. T. Sawyer (eds.), *Oxygen Complexes and Oxygen Activation by Transition Metals,* Plenum, New York, 1988, pp. 25–26.

23 R. E. Hester and E. M. Nour, *J. Raman Spectrosc., 11* (1981) 35.

24 (a) C. Walling, M. Kurz and H. Schugar, *J. Inorg. Chem., 9* (1970) 931; see also ref. 20.

25 L. Que and A. E. True, *Prog. Inorg. Chem., 38* (1990) 97–200.

26 S. J. Lippard, H. J. Schugar and C. Walling, *Inorg. Chem., 6* (1967) 1825.

27 (a) H. J. Schugar, C. Walling, R. B. Jones and H. B. Gray, *J. Am. Chem. Soc., 89* (1967) 3712; (b) H. J. Schugar, G. R. Rossman, C. G. Barraclough and H. B. Gray, *J. Am. Chem. Soc., 94* (1972) 2683.

28 A. O. Hill and D. G. Tew, in G. Wilkinson, R. D. Gillard and J. A. McCleverty (eds.), *Dioxygen, Superoxide and Peroxide, Comprehensive Coordination Chemistry,* Vol. 2, Pergamon, New York, 1987, pp. 315–333.

29 (a) B. A. Brennan, Q. Chen, C. Juarez-Garcia, A. E. True, C. J. O'Connor and L. Que, *Inorg. Chem., 30* (1991) 1937.

30 R. G. Wilkins and R. E. Yelin, *Inorg. Chem., 8* (1969) 1470.

31 F. J. Kristine and R. E. Shepherd, *J. Am. Chem. Soc., 99* (1977) 6562.

32 R. E. Shepherd, W. E. Hatfield, D. Stout, D. Ghosh and F. J. Kristine, *J. Am. Chem. Soc., 103* (1981) 5511.

33 F. J. Kristine, *Ph.D. Thesis,* University of Pittsburgh, 1980.
34 (a) M. Orhanovic and R. G. Wilkins, *Croat. Chem. Acta, 39* (1967) 149; (b) V. Zang and R. van Eldik, *Inorg. Chem., 29* (1990) 4462; (c) M. D. Lind, M. J. Hamor, T. A. Hamor and J. L. Hoard, *Inorg. Chem., 3* (1964) 34; (d) T. K. Myser and R. E. Shepherd, *Inorg. Chem., 26* (1987) 1544.
35 D. C. Harris, *Quantitative Chemical Analysis,* Freeman, New York, 1987, pp. 258–259.
36 G. McLendon, R. J. Motekaitis and A. E. Martell, *Inorg. Chem., 15* (1976) 2306.
37 (a) R. D. Lorentz, A. Bino and J. E. Penner-Hahn, *J. Am. Chem. Soc., 108* (1986) 8116; (b) A. Ardon and A. Bino, *Inorg. Chem., 24* (1985) 1343; (c) A. Bino and D. Gibson, *Inorg. Chem., 23* (1984) 109.
38 A. Bino and D. Gibson, *J. Am. Chem. Soc., 104* (1982) 4383.
39 J. Silverman and R. W. Dodson, *J. Phys. Chem., 56* (1952) 846.